

# Segmentation of Abdominal Aortic Aneurysm Using Deformable Models

*Marko Subasic, Domagoj Kovacevic, Sven Loncaric,  
Erich Sorantin\**

Faculty of Electrical Engineering and Computing,  
University of Zagreb

\*Radiology Department, University Hospital in Graz

## *Abstract:*

*We present the work that has been done on segmentation of abdominal aortic aneurysm (AAA) by Image Processing Group on Faculty of Electrical Engineering and Computing in Zagreb. We investigated performance of two types of deformable models: parametric and geometric deformable models both operating on three-dimensional data sets obtained by computer tomography angiography (CTA). Both inner and outer aortic borders can be segmented. The segmentation of the inner aortic border is trouble-free due to a contrast agent inside blood flow, which results in good image contrast on the inner aortic boundary. Segmentation of the outer aortic border presents a challenge because of poor image contrast on it. Tissue and organs surrounding the aorta can have similar optical density as aortic wall and that can make border between them hard to detect. Two types of deformable models provide two different solutions to the problem. Both segmentation methods have been tested on real patient data.*

## **1 Introduction**

Abdominal aortic aneurysm (AAA) [2], [6] is a vascular disease, which affects about 2% of people older than 65 years. AAA is an enlargement of the abdominal aorta due to weakened aortic wall. If left untreated AAA will enlarge over time increasing the risk of aortic wall rupture. As a fatal consequence 70 - 90% of patients with ruptured AAA will die. Although AAA can be imaged by plain abdominal films, ultrasound, computed tomography, magnetic resonance tomography [7] the gold standard is represented by intraarterial digital subtraction angiography. The information on aortic size and shape is of great importance in diagnostics, procedure planning and condition tracking. This information can be acquired from computer model of abdominal aorta, which can be obtained through imaging and image segmentation. Modern medical imaging techniques followed by appropriate image analysis methods [1] have shown to be useful for measurements of AAA [4], [8].

In this paper we describe two 3-D segmentation techniques based on deformable models, that we applied on segmentation of AAA. First technique utilizes manual segmentation of several slices (preferably on slices where significant change of aortic shape starts) followed by active contour-based automatic segmentation. Second technique utilizes manual initialization of deformable model (minimal user intervention is required) followed by automatic segmentation based on a level-set deformable model. The motivation behind our work is the need of accurate automatic segmentation which would relieve human experts of difficult and tedious manual segmentation and the need of high segmentation reproducibility.

## 2 Active contour approach

This approach is a trade off between fully manual methods which offer best results, but are time consuming and automatic methods which work with minimal interference from the operator, but offer less accurate results. The user is required to manually segment several slices along the aorta. Best results are obtained if the user manually segments slices where significant change in aortic shape occurs. Contours on those slices remain fixed. For the remaining slices initial contours are linearly interpolated. After initialization, active border algorithm is applied.

### 2.1 Active border algorithm

Active border is an extension of the active contour in 3-D space. In 3-D active border paradigm the algorithm attempts to minimize an energy function, which is a function of the optical density of the voxels on which the border is positioned and a function of the shape of the border. Border  $C$  is described by a parametric description [3] as shown in Equation 1.

$$C(s, r) = [X(s, r), Y(s, r), Z(s, r)]^T, \quad 0 \leq s \leq 1, 0 \leq r \leq 1 \quad (1)$$

The energy function is defined as  $E(C) = S(C) + P(C)$ , where  $S(C)$  is the external energy term (function of the image data) and  $P(C)$  represent the internal energy based on the shape of the border.

The function  $S(C)$  relates image data and deformable border.  $S(C)$  is based on an energy function  $V(x, y, z)$ , which is defined on all image data (Equation 2).

$$S(C) = \int_0^1 \int_0^1 V(C(s, r)) ds dr \quad (2)$$

The energy function  $V(x, y, z)$  should be formed in such a way to have low values for voxels that are likely to be border voxels of the desired structure. The purpose of the energy function  $P(C)$  is to ensure that border remains continuous and smooth. In our application we used discrete parametric description of border  $C$  as shown in Equation 3. We defined  $Z(s, r) = r$

and the value is kept constant for all nodes. The force is not calculated in  $z$  direction, which reduces 3-D surface to a set of 2-D curves that cannot move among slices.

$$C(s, z) = [X(s, r), Y(s, r), z]^T, \quad s \in \{s_0, s_1, \dots, s_m - 1\}, z \in \{z_0, z_1, \dots, z_n - 1\} \quad (3)$$

$$X^{n'} = X^{n-1} - \tau F_x(C^{n-1}), \quad Y^{n'} = Y^{n-1} - \tau F_y(C^{n-1}) \quad (4)$$

$$F_x = k_f \frac{|V^x|}{|V^x| + |V^y| + \epsilon} \quad (5)$$

Influence of  $S(C)$  on new node coordinates is calculated according to Equation 4 where  $\tau$  is discretization step and  $F$  is a force in  $x$  or  $y$  direction. The Equation 5 shows how  $F_x$  is calculated ( $F_y$  is calculated in similar way). Here  $k_f$  is a force constant,  $V^x$  and  $V^y$  are derivations of the function  $V(x, y, z)$  in appropriate directions and  $\epsilon$  is a small constant which ensures that there is no division by zero. Influence of the energy function  $P(C)$  is included through convolution of node coordinates ( $X^{n'}, Y^{n'}$ ) by two smoothing kernels along the curve and between curves (in  $z$  direction).

## 2.2 Implementation details

The energy function  $V(x, y, z)$  is calculated according to Equation 6,

$$V(x, y, z) = -G_{\sigma 2} \cdot \exp \left( - \left( \frac{D(x, y, z) - mg_z}{c_1 sg_z} \right)^2 - \left( \frac{I(x, y, z) - md_z}{c_2 sd_z} \right)^2 \right) \quad (6)$$

where  $I(x, y, z)$  is optical density of the original voxel,  $D(x, y, z) = |\nabla G_{\sigma 1} \cdot I|$  is image gradient calculated on a single slice ( $G_{\sigma 1}$  is a 2-D Gaussian kernel). For each of the manually segmented slices mean value and standard deviation of the gradient ( $mg_z$  and  $sg_z$ ) and of the optical density ( $md_z$  and  $sd_z$ ) are calculated on the border nodes. For slices which are not manually segmented mean and standard deviation values are linearly interpolated. The constants  $c_1$  and  $c_2$  are here to set weight of the gradient  $D$  and the optical density  $I$ , respectively. The above described deformable model algorithm stops if change in energy function falls below a predefined threshold.

## 2.3 Experimental results

The program has been tested in the clinical environment on the real patient abdominal CTA data. Segmentation was performed on the manually selected regions of interest extracted from the original CT volumes. Visualizations of the force functions are shown in Figures 1(a) and 1(b) and the result of the segmentation is shown in Figure 1(c). The smoothing kernels acting as internal force  $P(C)$  were constructed in a way to produce relative high smoothing and thus a very rigid deformable model. This however does not present a problem due to extensive and precise model initialization done by the user. This also enables the deformable model to successfully segment aortic aneurysm even when heavy image artifacts are present due to metal parts of prosthetic device.



(a) Forces along  $x$  direction

(b) Forces along  $y$  direction

(c) Segmentation results

**Figure 1: Active contour approach**

### 3 Level-set approach

This approach was an effort to produce fully automatic segmentation method which would require minimal user intervention. User intervention is used only to initialize the deformable model by placing a sphere inside the aorta. This is done by clicking on the sphere center and dragging the radius. We utilize a 3-D version of the level-set deformable model described in [9].

#### 3.1 Level-set algorithm

In the 3-D level-set algorithm, a 3-D surface of deformable model is represented as a set of points where 3-D function  $\Psi$  has the value (level) equal to zero. The function  $\Psi$  is defined as  $\Psi(\mathbf{x}, t = 0) = \pm d$ , where  $\mathbf{x} \in R^3$  and  $d$  is a distance from point  $\mathbf{x}$  to the given 3-D surface. Once initialized, the function  $\Psi$  is evolved through partial differential Equation 7. Discrete form, shown in Equation 8, is used in computations.

$$\frac{\partial \Psi(x, t)}{\partial t} + F|\nabla \Psi| = 0 \quad (7)$$

$$\Psi_{ijk}^{n+1} = \Psi_{ijk}^n - \Delta t F |\nabla_{ijk} \Psi_{ij}^n| \quad (8)$$

$$F = e^{-|\nabla G_{\sigma} * I_{ijk}|} (F_0 + F_1(K_{ijk})) \quad (9)$$

Here  $\Psi_{ijk}^n$  is value of function  $\Psi$  on coordinates  $(i, j, k)$  in  $n$ -th iteration. Speed factor  $F$  (Equation 9) consist of constant speed term  $F_0$ , curvature ( $K$ ) dependant term  $F_1(K)$ , and stopping factor  $e^{-|\nabla G_{\sigma} * I|}$  based on image gradient. Stopping factor of this form, stops deformable model on points with high image gradient.

While the basic level-set algorithm performs well on inner aortic border, outer aortic border poses a problem. Tissue surrounding aorta has similar optical density. If the neighboring

tissue touches aorta, then it is very difficult to distinguish border between them. The level-set deformable model relies heavily on image gradient on the border and if the gradient would be too small the deformable model would penetrate into surrounding tissue. This has shown to be the biggest problem in segmentation of aortic aneurysm using the level-set deformable model. To overcome the problem we introduced some knowledge based preprocessing. We utilized knowledge of aortic shape and distribution of voxel values. The preprocessing is aimed to enhancement of weak aortic borer and reconstruction of non existent aortic border. The preprocessing also has to eliminate high image gradient on inner aortic border that would interfere with segmentation of the outer aortic border. More details on used preprocessing can be found in [5]

### 3.2 Experimental results

The program has been tested on abdominal CTA data of 11 patients. Segmentation was also performed on the manually selected regions of interest extracted from the original CT volumes. The results have been compared to two result sets of manually corrected segmentations. The error was calculated as number of falsely segmented voxels on each CT slice. The average relative errors (from all segmented slices) between proposed algorithm and two sets of manually corrected results were 12.35% and 19.75% while the average relative error, between two manually corrected results, was 14.71%. The correlation of aortic surface on all slices was 0.93 and 0.91 compared to two manually segmented results. Figure 2(c) shows results for segmentation of outer aortic border. Large boundary gap on outer aortic border can be observed on gradient image Figure 2(b) as well as high image gradient on inner aortic border.

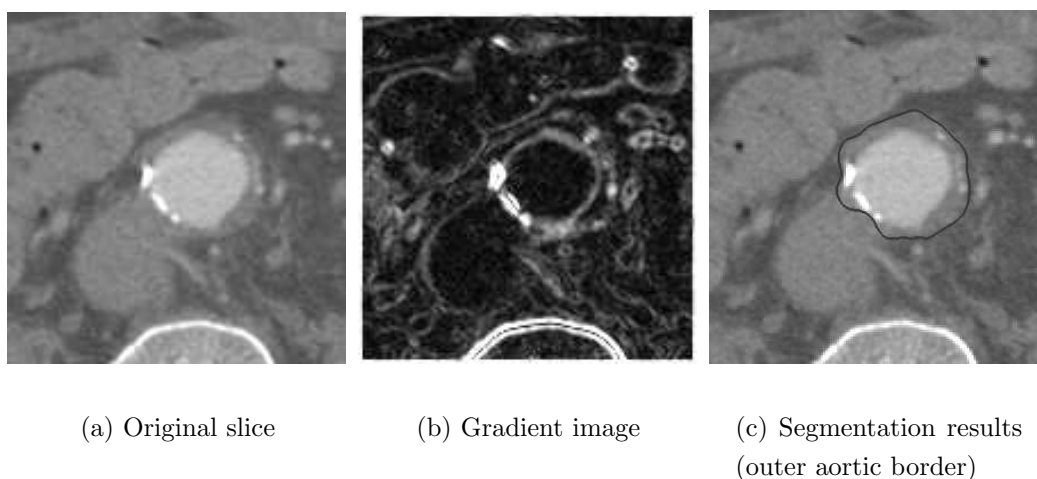


**Figure 2: Active contour approach**

## 4 Conclusion

We have tested two types of deformable models on segmentation of the abdominal aortic aneurysm. The methods have been tested in clinical environment. Both deformable models have been tested on real patients data and have shown good results. Two methods try to solve the segmentation problem from two different angles with different trade-off levels between the amount of user interaction and robustness. Active contour approach requires more user assistance but it is more robust and performs well even in atypical cases. The level-set approach requires minimal user interaction but it is more sensitive to image conditions. To eliminate negative influence of poor image contrast on outer aortic border, knowledge based image preprocessing has been proposed. This preprocessing improves the performance of the level-set deformable model.

## References

- [1] S. Juvvadi A. P. Dhawan. Knowledge-based analysis and understanding of medical images. *Computer Methods and Programs in Biomedicine*, 33:221–239, 1990.
- [2] C. B. Ernst. Abdominal aortic aneurysms. *New England Journal of Medicine*, 328:1167–1172, 1993.
- [3] I. Cohen L. D. Cohen. Finite-element methods for active contour models and balloons for 2d and 3d images. In *IEEE Transactions on Pattern Analysis and Machine Intelligence*, volume 15, pages 1131–1147, 1993.
- [4] R. Collorec C. Chardenon M. Garreau, J. L. Coatrieux. A knowledge-based approach for 3-d reconstruction and labeling of vascular networks from biplane angiographic projections. *IEEE Transactions on Medical Imaging*, 10:122–131, 1991.
- [5] E. Sorantin M. Subasic, S. Loncaric. 3-d image analysis of abdominal aortic aneurysm. In *Proceedings of SPIE Medical Imaging*, 2002.
- [6] M. N. Levy R. M. Berne. *Cardiovascular Physiology, 7th Ed.* Mosby-Year Book, 1997.
- [7] M. M. Thurnher F. W. Winkelbauer G. Kretschmer P. Polterauer J. Lammer S. A. Thurnher, R. Dorffner. Evaluation of abdominal aortic aneurysm for stent-graft placement: Comparison of gadolinium-enhanced mr angiography versus helical ct angiography and digital subtraction angiography. *Radiology*, 205:341–352, 1997.
- [8] E. Sorantin S. Loncaric, D. Kovacevic. Semi-automatic active contour approach to segmentation of computed tomography volumes. In *Proceedings of SPIE Medical Imaging*, volume 3979, 2000.
- [9] J. A. Sethian S. Osher. Fronts propagating with curvature dependent speed: algorithms based on hamilton-jacobi formulation. *Journal of Computational Physics*, 79:12–49, 1988.
- [10] D. Terzopoulos T. McInerney. Deformable models in medical image analysis: A survey. *Medical Image Analysis*, 1:91–108, 1996.